solids

MDPI

Article

Study of the Structure of Zn and Na Borophosphate Glasses Using X-ray and Neutron Scattering Techniques

Uwe Hoppe [1,*], Parker T. Freudenberger [2], Richard K. Brow [2], Jozef Bednarčik [3,†] and Alex C. Hannon [4]

[1] Institut für Physik, Universität Rostock, D-18051 Rostock, Germany
[2] Department of Materials Science and Engineering, Missouri University of Science and Technology, Rolla, MO 65409, USA; brow@mst.edu (R.K.B.)
[3] Deutsches Elektronen-Synchrotron DESY, D-22603 Hamburg, Germany; jozef.bednarcik@upjs.sk
[4] ISIS Facility, Rutherford Appleton Laboratory, Chilton, Didcot, Oxon OX11 0QX, UK; alex.hannon@stfc.ac.uk
* Correspondence: uwe.hoppe@uni-rostock.de
† Current address: Institute of Physics, Faculty of Science, Pavol Jozef Šafárik University, 040 01 Košice, Slovakia.

Abstract: The atomic structures of Zn and Na borophosphate glasses were studied using X-ray and neutron scattering techniques. Peaks assigned to the B−O, P−O, and O−O distances confirm that only BO_4 units co-exist with the PO_4 tetrahedra. The Zn−O and Na−O coordination numbers are found to be a little larger than four. The narrowest peaks of the Zn−O first-neighbor distances exist for the glasses along a line connecting the $Zn(PO_3)_2$ and BPO_4 compositions (50 mol% P_2O_5), which is explained by networks of ZnO_4, BO_4, and PO_4 tetrahedra with twofold coordinated oxygens. The calculated amounts of available oxygen support this interpretation. Broadened peaks occur for glasses with lower P_2O_5 contents, which is consistent with the presence of threefold coordinated oxygens. The two distinct P−O peak components of the Zn and Na borophosphate glasses differ in their relative abundances. This is interpreted as follows: Na^+ cations coordinate oxygens in some P−O−B bridges, which is something not seen for the Zn^{2+} ions.

Keywords: borophosphate glasses; short-range order; neutron scattering; X-ray scattering

check for updates

Citation: Hoppe, U.; Freudenberger, P.T.; Brow, R.K.; Bednarčik, J.; Hannon, A.C. Study of the Structure of Zn and Na Borophosphate Glasses Using X-ray and Neutron Scattering Techniques. *Solids* **2024**, *5*, 355–374. https://doi.org/10.3390/solids5030024

Academic Editor: Sophie Guillemet-Fritsch

Received: 26 April 2024
Revised: 7 June 2024
Accepted: 20 June 2024
Published: 1 July 2024

Copyright: © 2024 by the authors. Licensee MDPI, Basel, Switzerland. This article is an open access article distributed under the terms and conditions of the Creative Commons Attribution (CC BY) license (https://creativecommons.org/licenses/by/4.0/).

1. Introduction

The addition of B_2O_3 to phosphate glasses improves their chemical durability [1] and makes these glasses suitable for a variety of applications. Dissolution rates and thermal stability are optimized for biomedical use [2]. No tendency toward devitrification was observed in the rare-earth doped fibers of Na/Nb borophosphate glasses [3]. Borophosphate glasses with alkali modifiers are of particular interest due to their promising ionic conductivities and large glass-forming ranges extending into the P_2O_5- or B_2O_3-rich compositional regions [4]. The observation of maxima in ionic conductivity, for example, in the glasses $(A_2O)_{0.35}[(B_2O_3)_x(P_2O_5)_{1-x}]_{0.65}$ at x = ~0.4, gave rise to the introduction of the term mixed network-former effect [5] (A_2O—alkali oxide). A striking feature of the mixed glassy networks with compositions rich in P_2O_5 is that the boron forms exclusively tetrahedral BO_4 units with the corners mostly linked to phosphate tetrahedra but also to some neighboring BO_4 units [6–11]. The higher cationic mobility with increasing x is accompanied by increasing cross-link densities of the borophosphate networks. At the B_2O_3-rich end, the BO_4 fractions decrease, replaced by BO_3 units, to those values known according to the boron anomaly of binary alkali borate glasses [12].

The BO_4 formation in the P_2O_5-rich glasses with predominantly B−O−P bridges in the tetrahedral corners expresses the usual effect of additional oxygen in the phosphate networks, namely the disruption of P−O−P bridges [13]. The BPO_4 crystals [14,15] illustrate the mutual benefit for the PO_4 and BO_4 tetrahedra. They possess balanced valences of 1.25 and 0.75 vu (valence units) in their four bonds with P−O and B−O bond

lengths of ~0.152 and ~0.147 nm, respectively. The few known borophosphate crystals, e.g., $Na_3BP_2O_8$ [16], $Na_5B_2P_3O_{13}$ [17], and $Zn_3BO_3PO_4$ [18], have structures where the phosphate networks are already fully dissolved (no P−O−P bridges). Crystalline analogs for the glassy borophosphate networks are missing in the regions of samples that are rich in P_2O_5.

The present work aims to clarify the structural role of ZnO in the borophosphate networks and compare that role to the one played by Na_2O in two similar compositions. The glass-forming range of binary ZnO-B_2O_3 glasses is small [19] and ternary glasses with small P_2O_5 contents (<30 mol%) are difficult to obtain [13,20–22]. Raman spectroscopy, X-ray photoelectron spectroscopy (XPS), high-pressure liquid chromatography (HPLC), and ^{31}P or ^{11}B MAS NMR have provided detailed information on the structural evolution of the Zn-borophosphate networks whose chemical compositions are given in Figure 1a. B−O−B bridges alongside P−O−P bridges contradict the usual scheme of fully depolymerized phosphate networks [23]. This behavior was explained by the stronger acidity of the glass-former B_2O_3 [13], when compared, e.g., with Al_2O_3 in phosphate networks [24]. Most studies on the mixed network-former effect use a series of constant modifier contents, [6,10,11] as shown in Figure 1a. Other series have fixed O/P ratios, e.g., for the Zn alumino- and borophosphate glasses [13,24]. The O/P ratios determine the mean number of PO_4 corners in P−O−P bridges provided that all oxygen belongs to at least one PO_4.

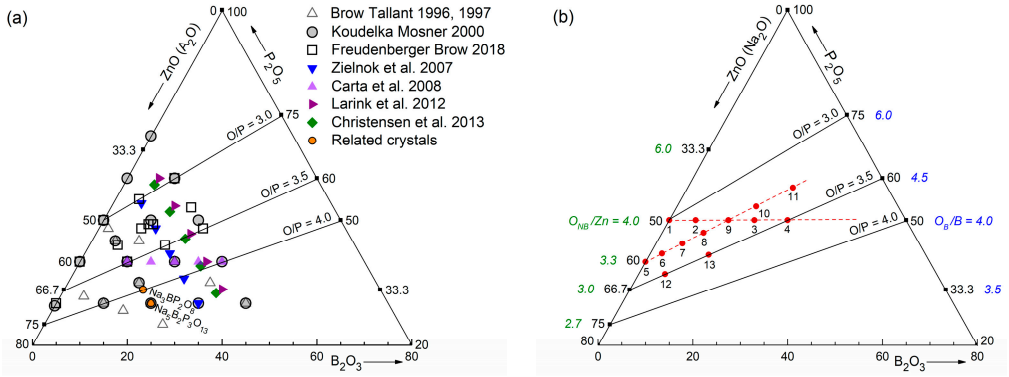

Figure 1. Compositions of the ternary zinc and alkali borophosphate glasses as reported in the literature (**a**) and measured in this work (**b**). The upper three citations [13,20–22] in (**a**) belong to ZnO-B_2O_3-P_2O_5 glasses, and the others [6,7,10,11] to alkali (A_2O) borophosphate glasses. The red dots with numbers in (**b**) mark the Zn borophosphate glasses of the present work. In addition to the ZnO and P_2O_5 contents, the O_{NB}/Zn and O_B/B ratios for the binary samples are given. Borophosphate glasses of compositions 8 and 13 with Na_2O instead of ZnO were also measured.

For describing the borophosphate networks, the labels P^n_{mB} and B^n_{mP} were introduced to describe the PO_4 and BO_4 (BO_3) units with the bridges P−O−P, B−O−B, and P−O−B [6–8]. The superscript n is the total number of bridging corners of the P- or B-centered units, while the subscript m gives the number of heteroatomic bridges. The corresponding fractions of groups can be widely resolved by ^{31}P and ^{11}B MAS NMR [6–11] and were useful for developing quantitative descriptions of the compositional dependence of the network structures. These models, however, are not used to analyze the Zn- and Na-centered oxygen polyhedra in the borophosphate glasses, which is the focus of the present work. Here, the critical parameter will be the number of P−O bonds that do not link to neighboring PO_4 tetrahedra, which will ultimately determine the coordination environments of the Zn- and Na-ions. Therefore, besides the P^n_{mB} and B^n_{mP} units, the PO_4 units will still be characterized by the common Q^n nomenclature, where the superscript n gives the number of PO_4 corners in P−O−P bridges with possible n = 3, 2, 1, or 0 [23]. The oxygens of binary phosphate glasses are divided into O_B (bridging in P−O−P) and O_{NB} (non-bridging in other bonds). In detail, the O_B atoms of the borophosphate glasses can form P−O−P, P−O−B, and B−O−B bridges, where some of them have modifier cations in their vicinity.

A complete description of all combinations of nearest neighbors is a challenging task. The knowledge of the binary systems is helpful to start.

In binary $(ZnO)_x(P_2O_5)_{1-x}$ glasses with $0.33 \leq x \leq 0.5$, the Zn−O coordination number (N_{ZnO}—the number of oxygens surrounding a Zn site) decreases from six to four with increasing zinc oxide content [25–27]. The minimum N_{ZnO} of four is reached at 50 mol% P_2O_5 [28]. In this compositional range, the N_{ZnO} value follows the O_{NB}/Zn ratio = $2/x$, indicating real Zn−O−P bridges [25]. The O_{NB}/Zn ratio of the binary system is given on the left axis of Figure 1b. For glasses with $x > 0.5$, increasing fractions of O_{NB} must share two Zn neighbors. The P−O_{NB} bonds of the Q^n with n = 3, 2, 1, and 0 show decreasing bond valences with 2.0, 1.5, 1.33, and 1.25 vu (valence unit) [23]. Thus, the electron charges on the O_{NB} increase, and are to be balanced by the Zn-ions. The Q^1 and Q^0 groups supply a sufficient charge to their O_{NB} to be shared by two Zn^{2+} that still form ZnO_4. The bond valence is not strictly fixed for a given P−O_{NB} in a Q^n. The P−O_{NB} bond distances show variations according to the demands of their local environments. For example, the bond valence P−O_{NB} of the Q^3 is a little less than 2.0 vu if this O_{NB} coordinates a Zn [26]. For $x > 0.5$, the O_{NB} atoms shared by two Zn cause some elongated Zn−O bonds if compared with those in Zn−O−P bridges. This effect broadens the peak of Zn−O distances. Also, the Zn−O coordination can exceed the number four in the binary glasses of the phosphate-rich compositions ($x < 0.5$) [29]. A broadening of the Zn−O peaks is expected, as well, because of longer bonds associated with the ZnO_5 or ZnO_6 that account for the increasing $N_{ZnO} > 4$ [25–27].

This work will mainly focus on the variations in the Zn−O distance peaks; the P and B environments and the borophosphate networks were characterized in a preceding work [13]. In addition to the glasses along a line from $Zn(PO_3)_2$ to BPO_4 with fixed 50 mol% P_2O_5, two series with fixed O/P ratios are chosen for the diffraction study. An earlier measured sample of a binary Zn borate glass is adopted for discussing the change in the ZnO_m units for a glass being free of P_2O_5. Two additional samples contain Na_2O instead of ZnO to investigate the different effects of the Na^+ and Zn^{2+} cations on details of the P−O bond lengths.

2. Materials and Methods

2.1. Samples

The zinc borophosphate glasses were prepared as described in a preceding work (Freudenberger and Brow [13]). The raw materials ZnO (99.5+%, Acros Organics, Waltham, MA USA), H_3BO_3 (cer. ACS, Fisher Scientific, Rochester, NY USA), and H_3PO_4 (85%, Fisher) were mixed to obtain glasses with the nominal compositions as given in Figure 1b and Table S1 (Supplementary Material). The samples are labeled zbp01 and so on according to their numbers given in Figure 1b. Two Na borophosphate glasses with labels nbp08 and nbp13 were prepared using Na_2CO_3 (99.5%, Alfa Aesar, Ward Hill, MA USA) as a raw material. The mixtures were calcined in platinum crucibles for 16 h at 350 °C. The duration of melting was two hours at temperatures in the range of 1000–1225 °C. The melts were quenched in preheated carbon molds. The clear glasses were annealed for one hour at temperatures of 400–550 °C (each at 10 °C below the respective glass transition temperature) [13]. The chemical analyses of the Zn borophosphate glasses of the preceding study [13] gave a loss of P_2O_5 content from 0 to 6 mol% with uncertainties of ~2.5 mol%. It was decided to start the data analyses with the batch compositions. The mass densities were measured using the Archimedes method. Two samples (zbp04, zbp11) exceed the range of homogeneous glasses that was reported in [22].

2.2. X-ray Scattering

The X-ray scattering (XRD) experiments were performed at the synchrotron (storage ring PETRA III at DESY Photon Science Hamburg/Germany). The hard photons at the beamline P02.1 have fixed radiation energies of ~60 keV. The exact wavelength of the incident beam (0.02080 nm) and the sample–detector distance (249.9 mm) were calibrated

with the diffraction pattern from CeO_2 powder. The beam size was 0.5 × 0.5 mm^2. Thus, the beam is narrower than the silica capillaries (diameter 1 mm and wall thickness ~10 µm) that contain the powdered sample material. The beam stop between the sample and detector was fixed on a Kapton foil. The image-plate detector (Perkin Elmer 1621; Perkin Elmer Optoelectronics, Wiesbaden, Germany) used in these experiments is sensitive to photons of radiation energies > 20 keV. The samples were irradiated five times for one second with a full duration of the measurement equal to one minute per sample. The two-dimensional scattering images were merged to functions of the scattering angle 2θ. Further details on the instrument and first data analysis are described elsewhere [30]. The scattering intensities were corrected for container scattering, background, and absorption. The final intensities $I_{corr}(Q)$ were normalized to the structure-independent scattering, which makes use of the chemical compositions of the samples and the tabulated atomic data of coherent and Compton scattering $I_{compt}(Q)$ [31,32]. The final X-ray structure factors $S_X(Q)$ are given by the following:

$$S_X(Q) = \left[I_{corr}(Q) \cdot N - < f^2(Q) > - I_{compt}(Q) \right] / < f(Q) >^2 \quad (1)$$

where <. . .> means the average of the sample composition and $f(Q)$ is the coherent atomic scattering amplitude. The normalization factor N allows $S_X(Q)$ to oscillate around unity. Smoothly changing corrections improve the behavior in the upper end of the Q-range. The scattering data of the zbp14 sample were obtained in an earlier laboratory experiment using Ag K_α radiation. A recent work [19] improved the knowledge of the range of binary Zn borate glasses from 54 to 70 mol% ZnO. Glasses with a smaller ZnO content show the separation of a B_2O_3-rich phase during melting. The Raman spectrum of the clear part of the glass with a 50 mol% batch is identical to that of the 54 mol% glass [19]. Hence, 54 mol% ZnO is also used for analyzing the data of the zbp14 sample instead of its batch composition of 50 mol%.

2.3. Neutron Scattering

The neutron scattering experiments were performed using the GEM instrument of the neutron spallation source ISIS of the Rutherford Appleton Laboratory (Chilton/UK). Measurements were made for six of the fifteen samples (zbp05, zbp07, zbp09, zbp11, zbp13, nbp13). The powdered sample material was loaded into thin-walled vanadium cylinders (diameter: 10.33 mm for all samples). The cylinder wall is a vanadium foil which is only 0.025 mm thick. The duration of data acquisition was at least 5 h per sample. A vanadium rod was used to determine the incident energy spectrum that is needed for the data normalization in the time-of-flight regime. The data were corrected using standard procedures for container and background scattering, attenuation, multiple scattering, and inelasticity effects [33]. Since natural boron with 20% of the strongly absorbing isotope ^{10}B was used, a strong wavelength-dependent neutron absorption occurs. The corrections proved to be reliable even for up to 8% of boron atoms in the zbp11 sample. The differential scattering cross-sections of the detector groups 2, 3, 4, and 5 (scattering angles 14°–109°) are normalized to the mean scattering that is calculated from the sample compositions and tabulated neutron scattering lengths. Finally, the neutron structure factors $S_N(Q)$ were obtained in analogy to Equation (1).

3. Results

The corrected and normalized X-ray structure factors of the borophosphate glasses are shown in Figure S1. The $S_X(Q)$ data of the samples zbp04 and zbp11, which are close to the border of glass formation [22], show small Bragg reflections of tiny crystalline fractions. Statistical noise is no issue in the measurements using image plates. The neutron scattering experiments of six samples cover large Q-ranges, which bears the advantage of an excellent real-space resolution. The neutron diffraction results are shown in Figure 2 by the interference functions, which are weighted by the factor Q. The experimental data are

compared with model curves composed of damped sinusoidal functions. These oscillating functions in the scattering intensities are the pendant to Gaussian peaks in the real-space correlation functions $T(r)$. The model curves are calculated by the parameters given in Table S2 as obtained from the subsequently described Gaussian fitting. The $T(r)$ functions are Fourier transforms of the experimental $S(Q)$ data with the following:

$$T(r) = 4\pi r\rho_0 + \frac{2}{\pi}\int_0^{Q_{max}} Q[S(Q) - 1]M(Q)\sin(Qr)dQ \ . \quad (2)$$

The number densities of atoms, ρ_0, are calculated from the mass densities and glass compositions given in Table S1. The $T(r)$ functions are calculated with Q_{max} = 183 nm^{-1} (X-rays), 400 nm^{-1} (neutrons), and $M(Q)$ = 1. According to Lorch, a damping $M(Q)$ with Q_{max} = 200 nm^{-1} (X-rays) and 500 nm^{-1} (neutrons) was used for a second series of $T(r)$ functions. The Gaussian fitting procedures of the first-neighbor peaks were applied to both series of $T(r)$ functions, where the effects of truncation at Q_{max}, $M(Q)$ damping, and the Q-dependence of the partial weighting factors in the case of X-rays are taken into account [34,35]. Good fits for the first-neighbor peaks were obtained for all X-ray $T(r)$ functions, whereas the fits of the Zn−O (Na−O) peaks in the neutron $T(r)$ functions were not as good for some cases. Several comparisons of the model $T(r)$ functions with the experimental $T(r)$ functions are exemplified in Figures 3, 4 and S2–S4. The resulting peak parameters are listed in Table S2.

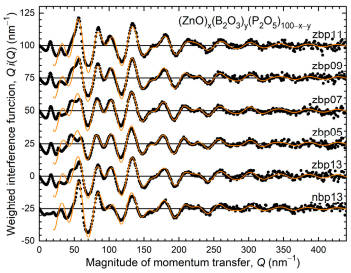

Figure 2. Weighted neutron interference functions, $Q\cdot[S(Q)-1]$: the experimental data (black dots) are compared with model functions (orange solid lines) that are calculated by the parameters given in Table S2 for the model first-neighbor peaks. Except for zbp13, the baselines of the data are shifted up or down for visual clarity.

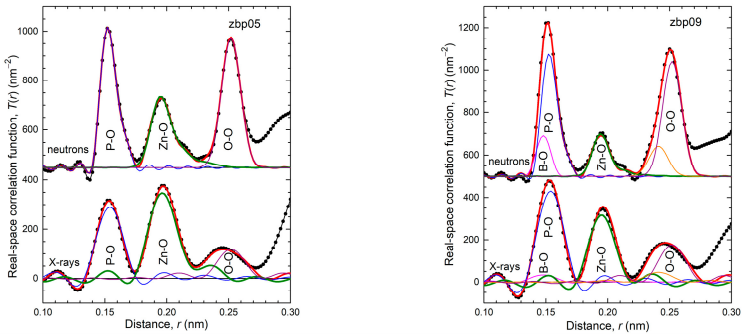

Figure 3. Neutron and X-ray correlation functions $T(r)$ of the zbp05 and zbp09 samples as obtained by Equation (2) without damping ($M(Q)$ = 1). The baselines of the neutron data are shifted up for visual clarity. The experimental curves (black dots) are compared with the total model functions (thick red lines) and the partial Zn−O peaks (thick olive lines). The other partial model peaks are given with thin lines (B−O—magenta; P−O—blue; O−O—orange and purple). The two model O−O peaks correspond to different edge lengths of the BO_4 and PO_4 tetrahedra.

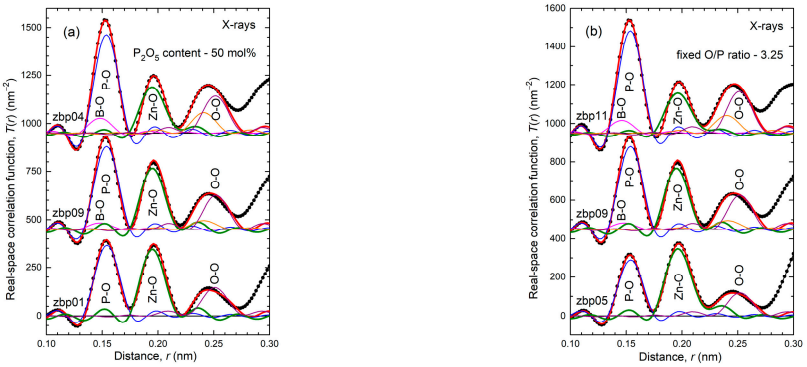

Figure 4. X-ray correlation functions $T(r)$ as obtained without damping ($M(Q) = 1$) for the series with fixed P_2O_5 content (**a**) and fixed O/P ratio (**b**). Except for zbp01 and zbp05 samples, the baselines of the data are shifted up for visual clarity. The experimental curves (black dots) are compared with the total model functions (thick red lines) and the partial Zn−O peaks (thick olive lines). The other partial model peaks are given with thin lines (B−O—magenta; P−O—blue; O−O—orange and purple). The two model O−O peaks correspond to different edge lengths of the BO_4 and PO_4 units.

The combination of X-ray and neutron scattering does allow the separation of the B−O and P−O bonds due to the different changes in scattering contrast. Nevertheless, $N_{BO} = 4$ was fixed in this analysis, which is consistent with previous ^{11}B MAS NMR studies that showed that BO_4 units were dominant in the structures of the full compositional range of the investigated borophosphate glasses [8,13,21,22]. In scattering experiments, the limit of detection for the presence of any BO_3 fractions is of poorer certainty (±10%). The bond length of 0.147 nm for the BO_4 is taken from related crystals [14–17] and is used together with a reasonable peak width to fit the scattering data.

For the binary ZnO-P_2O_5 glasses (zbp01, zbp05), the P−O peak is based on two bond lengths, P−O_{NB} and P−O_B, which differ by ~0.010 nm [26,36]. These fractions are directly determined from the P−O peaks in the $T(r)$ of zbp05 from neutron diffraction (Figure 3). The bond fractions are also calculated from the O/P ratio that corresponds to the average n of the Q^n distributions [23]. Here, the corresponding relation is also applied to the ternary glasses, assuming that the P−O bonds in P−O−B bridges are only insignificantly longer than those in P−O−Zn bridges. The necessary changes in the bond fractions to achieve excellent fits are small for the P−O peaks of all samples. However, the bond fractions calculated from O/P ratios are not correct for glasses with B−O−B bridges. Additional P−O−P bridges must also form [13]. The observed P−O bonds of the Na borophosphate glasses show slightly different behavior. Both deviations are discussed in Section 4.3.

Finally, the two P−O distances give a satisfactory approximation of the P−O peaks for all samples. Two samples show total N_{PO} values of 3.6, which differs from the expected 4.0 by more than the common uncertainty. That can be due to a slightly changed composition for the zbp11 sample because its N_{ZnO} appears quite large. The deviation for zbp06 must be due to a normalization problem. In the case of all other samples, the N_{PO} values are quite reasonable, which gives support to the use of the batch compositions for these analyses. The O−O peaks at 0.25 nm belong to the edges of the BO_4 and PO_4 units. The numbers of the tetrahedral edges were calculated from the fractions of the BO_4 and PO_4 units according to the batch compositions (Table S1). The calculation of the N_{OO} value of the Zn borate glass zbp14 takes into account the fractions of the BO_4 and BO_3 units according to $N_{BO} = 3.3$, which equals the result from ^{11}B MAS NMR [19]. The successful fits of the huge O−O peaks in the case of the neutron $T(r)$ functions support the choice of this approach. The edge length of the BO_4 tetrahedron was fixed to 0.241 nm as taken from a crystal [14], and that of the PO_4, which was close to 0.252 nm, was adjusted a little for each case.

Good fits of the metal cation–oxygen distances are possible up to ~0.27 nm. That is the lower limit of the B−O, P−O, and O−O second-neighbors with unknown numbers and distances. The overlaps with the O−O distances of the BO_4 or PO_4 tetrahedral edges

are no issue in the fits. The contrast change of X-ray and neutron scattering differs for the O−O and Zn−O (Na−O) correlations. In addition, the calculated O−O peaks gave reasonable fits.

The scattering weight of the Zn−O partial correlation is larger for X-rays than for neutrons. Therefore, $T(r)$ fitting in the range of the Zn−O distances was made to the X-ray correlation functions independent of the neutron data. The high-energy XRD has several advantages, including low absorption, and thus little demand for precise sample positioning. On the other hand, the real-space resolution of the neutron data is so good that termination effects are nearly vanishing. Oscillations caused by termination at Q_{max} in Equation (2) are visible only for the narrow B−O and P−O peaks, but not for the others (cf. Figure 3). The positions and shapes of the obtained Zn−O peaks are reproduced in the neutron data. The full peak heights are not reached for the zbp11 and zbp13 samples (Figure S3). The Zn−O partial of zbp11 has a small scattering weight for neutrons (only 5%) and large corrections for the highly absorbing boron content were needed. It is noteworthy that the fits to the $T(r)$ functions obtained with Lorch damping gave equivalently good results. Figure S4 shows both variants of fits for the sodium borophosphate glass nbp13. The Na−O distances overlap with the O−O peaks. The X-ray data show a good fit for the broad Na−O peak with four oxygen neighbors at distances centered at 0.238 nm (Table S2). The neutron $T(r)$ functions show unphysical features at ~0.185 nm, as indicated in Figure S4.

The present work aims to clarify how the glass composition affects the Zn−O environment. At first glance, the results are disappointing in that interesting changes are not observed. The Zn−O coordination numbers given in Figure S5 are almost constant at ~4.4, showing a slight increase toward smaller ZnO contents. The N_{ZnO} values of zbp06 and zbp11 are considered outliers. It is noteworthy that these are also the samples with small N_{PO} values = 3.6. Commonly, the bond lengths increase with N_{ZnO} and the mean distances can be used as a criterion for the N_{ZnO} values. The ZnO_4, ZnO_5, and ZnO_6 units have mean bond lengths of 0.194, 0.205, and 0.209 nm, respectively, as found in related crystal structures [37–39]. The Zn−O distances in the glasses have been reported with 0.194 nm for ZnO_4 [28] and 0.209 nm for ZnO_6 units [26]. In the present work, the Zn−O distances vary from 0.196 to 0.199 nm, with changes only a little outside the uncertainty interval (cf. Figure 5); these lengths were consistent with the obtained coordination numbers, which were found to be a little larger than four. A careful inspection of the bond lengths of the series with constant O/P = 3.25 (Figure 5b) identifies the shortest bonds for the zbp09 sample. This sample is also a member of the series of constant 50 mol% P_2O_5 (Figure 5a), where systematic distance changes were not observed. The Zn borate glass (zbp14) has an N_{ZnO} value of 4.3 and the largest detected Zn−O bond length of all samples at 0.200 nm (cf. Table S2). The Gaussian fit of this sample was repeated using the batch composition of 50 mol% ZnO instead of the 54 mol% taken from [19]. The two N_{ZnO} values do not differ, which is explained by a compensation of the compositional Zn decrease and O increase in the calculation of the Zn−O weighting factors. In the case of using 50 mol% ZnO, however, an N_{BO} of only 2.9 was obtained.

The Zn−O peaks in the total X-ray $T(r)$ functions (Figure 4) do not show significant changes. A further way to compare them is by considering the model peaks, which are here presented by the radial distribution functions. These Zn−O model peaks were calculated with the parameters obtained from Gaussian fitting and these peaks are compared with the bond lengths in the related crystals. This approach was recently used for binary phosphate glasses [27], where it was shown that the termination effects of the Fourier transformation (broadening and oscillations) and the influence of the changed scattering weights as the ZnO content changes are widely eliminated. The full widths at half maximum (fwhm) of these model peaks are shown in Figure 6. Again, a minimum is found for the zbp09 sample in the series in Figure 6b, whereas the values in Figure 6a do not show any clear trend. The Zn−O model peaks of all samples are shown for the three series of constant P_2O_5 content or constant O/P ratio (cf. Figure 7). For better comparability, the peaks of the glasses

are given with identical heights. The peaks of the ZnO_4, ZnO_5, and ZnO_6 units from the crystals show significant differences in the bond lengths. For all three series, the peaks of the glasses are close to that of the ZnO_4 units known from the β-ZnP_2O_6 crystal [37]. The ZnO_4 polyhedron of β-ZnP_2O_6 has a fifth oxygen nearby. Hence, the small contributions at ~0.230 nm found for all samples can be interpreted as real distances. Significant differences exist at ~0.215 nm. The peaks of the glasses with a constant 50 mol% P_2O_5 content shown in Figure 7a have small numbers of such distances and change very little. The samples outside the line of 50 mol% (cf. Figure 1) have significantly more Zn−O bonds at ~0.215 nm as becomes visible in Figure 7b,c. The differences appear very pronounced for the samples shown in Figure 7c. The zbp12, zbp13, and zbp14 samples have visibly more distances at ~0.215 nm than zbp04, due to bond lengths that belong to fractions of ZnO_5 or ZnO_6 units or shared O_{NB}. This behavior is also found for zbp05, zbp06, zbp07, and zbp11 in Figure 7b. Among them, zbp11 is the only sample with a P_2O_5 content > 50 mol% (cf. Figure 1b). According to the large uncertainties of the measured coordination numbers, the behavior shown by the bond lengths is a better basis for discussing the Zn−O environments in the Zn borophosphate glasses. To support this statement, the fractions of the long bonds are calculated with $N_{long}/(N_{short} + N_{long})$ and given in Figure S6. The N_{short} and N_{long} values are the numbers of oxygen neighbors at 0.194 and ~0.212 nm, as given in Table S2. Similar to the fwhm in Figure 6, the N_{long} fractions for the series with constant 50 mol% P_2O_5 (Figure S6a) do not show systematic changes, whereas the minimum of long bonds in the series with the O/P ratio of 3.25 is found for the zbp09 sample (Figure S6b).

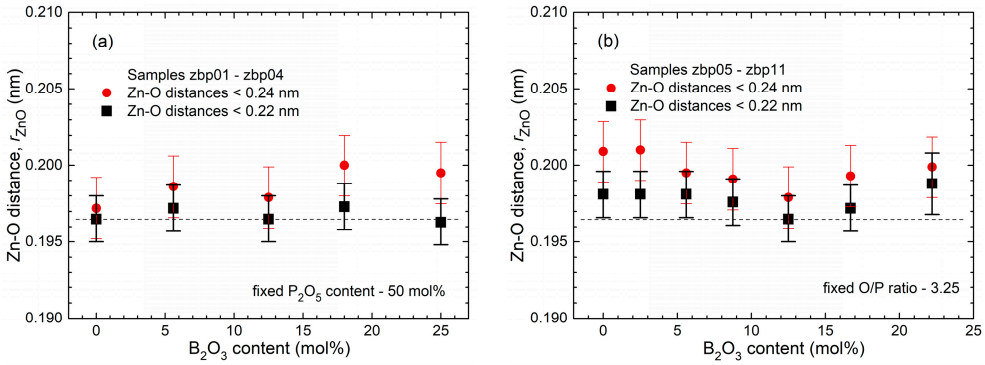

Figure 5. The Zn−O first-neighbor distances for two series of the Zn borophosphate glasses: (**a**) constant P_2O_5 content, (**b**) constant O/P ratio. The black squares denote the values corresponding to typical bond lengths. The red circles are values that include the contributions being a little longer with ~0.23 nm. To assign sample numbers, see Figure 1b. The equal values at 12.5 mol% B_2O_3 in (**a**) and (**b**) belong to sample zbp09.

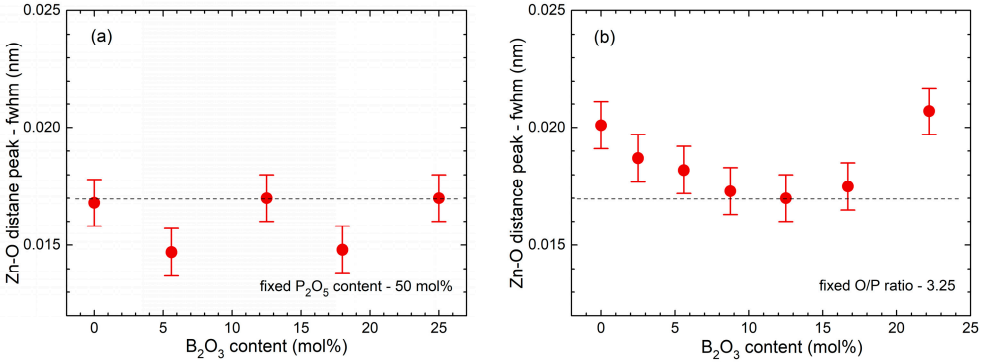

Figure 6. Full widths at half maximum (fwhm) values of the model Zn−O peaks as shown in Figure 7 for two series of the Zn borophosphate glasses: (**a**) constant P_2O_5 content, (**b**) constant O/P ratio. To assign sample numbers, see Figure 1b. The equal values at 12.5 mol% B_2O_3 in (**a**,**b**) belong to the zbp09 sample.

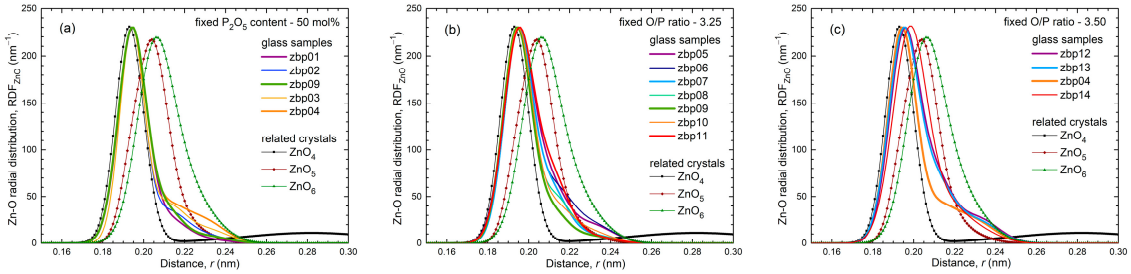

Figure 7. Model peaks of the Zn−O first-neighbor distances of the series with (**a**) constant P_2O_5 content, (**b**) constant O/P ratio of 3.25, and (**c**) constant O/P ratio of 3.5 as obtained from Gaussian fitting (solid lines). It is compared with peaks that are calculated for the ZnO_4, ZnO_5, and ZnO_6 units known of related crystal structures [37–39] (lines with symbols) and the peak of a binary Zn borate glass (zbp14). The model peaks of the glasses are given with identical heights and the changes in their widths become obvious.

4. Discussion

4.1. Fully Tetrahedral Networks and the Ratio O_{NB}/Zn

The Zn borophosphate glasses have the potential to form continuous disordered networks of corner-connected tetrahedra with all oxygen atoms being two-fold coordinated. The Zn metaphosphate glass (50 mol% P_2O_5) has been considered a continuous tetrahedral network for a long time now [40], which is manifested in its properties [41]. This classification is not entirely accurate because the Zn−O coordination number is slightly larger than four, which is also reflected in the corresponding bond lengths (Figures S4 and 5). The ZnO_4 units of the β-$Zn(PO_3)_2$ crystal [37] show a fifth Zn−O bond of 0.28 nm in length. Similarly, a few longer distances exist for the investigated glasses. Nevertheless, the metaphosphate glass zbp01 and the borophosphate glasses of 50 mol% P_2O_5 (zbp02, zbp09, zbp03, and zbp04) show the narrowest Zn−O peaks, together with the smallest distance contributions at ~0.212 nm (Figures 7a and S6); this is evidence that a great majority of Zn ions are in tetrahedral units that have their four corners in Zn−O−P linkages.

The Zn−O peaks of the samples possessing less than 50 mol% P_2O_5 show increased contributions at ~0.212 nm that indicate O_{NB} shared by two Zn. A significant increase in the corresponding N_{ZnO} is not detected. Two samples (zbp10, zbp11) of the series with the fixed O/P ratio of 3.25 have more than 50 mol% P_2O_5. The zbp11 sample shows significantly increased values of N_{ZnO}, r_{ZnO}, and peak width (fwhm). In this case, the O_{NB}/Zn ratio is larger than four, and some larger units than ZnO_4 are formed. Similar to the binary ZnO-P_2O_5 system [25,26,42], the borophosphate networks behave in such a way that avoids PO_4 units (Q^3, Q^2) with terminal P=O double bonds. The possible second bond partner of this oxygen is Zn but not B, for reasons of bond valences. This is in contrast to what has been found for the Zn aluminophosphate glasses, where the Al^{3+} cations form AlO_5 and AlO_6 units for the P_2O_5-rich and ZnO-poor compositions [24]. This structural flexibility of Al allows the glass-forming range to reach the binary Al_2O_3-P_2O_5 border. However, similar to the BPO_4, the range of the $AlPO_4$ composition is excluded for its strong crystallization tendency.

On the side of the binary B_2O_3-P_2O_5 system, BPO_4 crystals [14,15] are known, but disordered networks of PO_4 and BO_4 units are not formed. The structure of BPO_4 consists of P^4_{4B} and B^4_{4P} units, each connected via their four corners by P−O−B bridges. Figure 8a shows the bond valences in the BPO_4 crystals formed by these units. The tetrahedral network in the $Zn(PO_3)_2$ metaphosphate glass consists of P^2_{0B} and ZnO_4 units (Figure 8b). If one connects the $Zn(PO_3)_2$ and the BPO_4 compositions (50 mol% P_2O_5) in Figure 1, their mixture could create networks of ZnO_4, BO_4, and PO_4 units whose corners are connected exclusively by twofold coordinated oxygens. That behavior receives support from the narrow Zn−O distance peaks (Figure 7a). However, the question arises as to how the structures made of $Zn(PO_3)_2$ and BPO_4 with mixed P^2_{0B} and P^4_{4B} groups can be arranged, whereby the isolated ZnO_4 and BO_4 units must be provided with the necessary bond

valences. Starting from the side of the ZnO-rich glasses, the problem is solved using a structural speciation reaction:

$$P^2_{0B} + P^4_{4B} \leftrightarrow 2P^3_{2B} \quad (3)$$

where the oxygens of the P^3_{2B} (a Q^1 unit) are shared with one ZnO_4, one PO_4, and two BO_4 units, as shown in Figure 8c. The Q^1 groups terminate the phosphate chains. Most ZnO_4 corners interact with the remaining Q^2 groups while the BO_4 tetrahedra connect the Q^1 and Q^0 groups. Neither the ZnO_4 nor the BO_4 could exist in isolated sites alone with only Q^1 neighbors (with P^1_{0B} or P^4_{3B}, respectively). The ZnO_4 would have to share O_{NB} and the BO_4 would not receive sufficient bond valence. Approaching the composition of the zbp04 sample, nearly all Q^2 have changed to Q^1 groups. A high ordering of the ZnO_4 and BO_4 is required so that both groups can receive the necessary bond valences. Fortunately, a further solution exists for the bond valences, which stabilizes the disordered borophosphate networks, whereby some of the oxygens that, for example, would form P−O−B bonds, are instead incorporated into B−O−B bonds, necessitating the concomitant formation of new P−O−P bonds to produce a weak polymerization of the phosphate network [13]. This rearrangement is described by the following:

$$P^4_{4B} + B^4_{4P} \leftrightarrow P^4_{3B} + B^4_{3P}. \quad (4)$$

Figure 8d illustrates an arrangement of a P^4_{3B} with a B^4_{3P} unit. ^{11}B MAS NMR has determined the fractions of the B^4_{3P} in addition to the B^4_{4P} units [13]. Hence, the O/P ratio is no longer exactly related to the Q^n distribution. Four of the Zn borophosphate glasses used in [13] have ~50 mol% P_2O_5. The glass with the highest B_2O_3 fraction (18.5 mol%) was found with the highest B^4_{3P} fraction (88%). The other samples had ~35% B^4_{3P} in addition to the B^4_{4P} units. Reactions according to Equation (3) take place in glasses of high Q^2 fractions (high ZnO content), whereas reactions according to Equation (4) dominate when the Q^2 units are already in the minority (equal amounts of ZnO and B_2O_3). The fraction of oxygens that are available for coordinating the Zn^{2+} cations is preserved when the fraction of B^4_{3P} units changes. Equation (4) does not change the numbers of P−O and B−O bonds, as illustrated in Figure S7. That allows us to calculate the accurate O_{NB}/Zn without knowing the accurate B^4_{3P} fraction and this O_{NB}/Zn ratio largely determines the Zn−O environments.

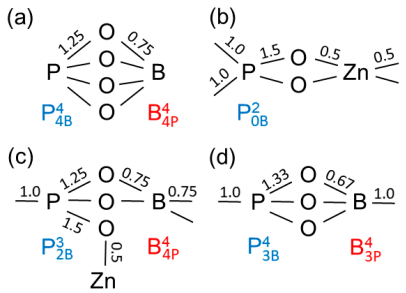

Figure 8. Schemes of the bond valence distributions in the PO_4, BO_4, and ZnO_4 units of fully tetrahedral networks: (**a**) BPO_4 crystal, (**b**) $Zn(PO_3)_2$ glass, (**c**) Zn borophosphate glass with P^3_{2B} and B^4_{4P} units, and (**d**) Zn borophosphate glass with P^4_{3B} and B^4_{3P} units. The numbers indicate the bond valences given in valence units (vu). Bond valences of 1.0 represent P−O−P or B−O−B bridges. The values of bond valences are not repeated for equivalent bonds.

Now, the question of how one can divide the oxygen fractions to coordinate the Zn and B is discussed. Simply knowing the sample composition of the ternary phosphate glasses is not sufficient for addressing this. The available number of oxygens is derived by subtracting the number of P−O−P bonds per PO_4 and that is calculated from the total O/P ratio. In analogy to the structural behavior of the Zn phosphate glasses (cf. Introduction), all oxygens will find two neighbors with decreasing P_2O_5 content (P, B, Zn) before threefold coordinated oxygen sites occur. Sophisticated considerations have to take into account the

different properties of the two sorts of cations besides the P^{5+} such as charge balance, field strength, preference of definite oxygen polyhedra, or threefold coordinated oxygen sites.

A general model (model 1) takes into account the different requirements for the charge compensation of the Zn^{2+} and B^{3+} cations. It is assumed that the two cationic species act independently of each other and are linked to the different Q^n with equal probability, which makes sense for a simple approach. The corresponding O_{NB}/Zn and O_B/B values are obtained with the following:

$$O_{NB}/Zn = 4(c_O - 2\,c_P)/(2c_{Zn} + 3c_B) \quad (5)$$

and

$$O_B/B = 6(c_O - 2\,c_P)/(2c_{Zn} + 3c_B) \quad (6)$$

where the c_i are the concentrations of the four sorts of atoms. This approach produces O_B/B ratios that are too large (>4) for all samples, as shown in Figure 9, where the ratios are considered for the series with constant P_2O_5 contents at 50 mol% (a) and constant O/P ratios of 3.25 (b). The boron cannot meet this coordination behavior. In other words, the Zn−O environments and BO_4 units cannot form independently of each other. Preferences for special Q^n neighbors, as shown in Figure 8c,d, must be effective. In the range of the glasses studied, the situation is quite simple because ^{11}B MAS NMR detected only BO_4 (no BO_3) [13]. When N_{BO} is fixed to the number four for BO_4 units, a well-defined fraction of oxygens is used as bridging oxygens by the borons. Then, the oxygens formed as non-bridging in the PO_4 units are used for the coordination of the zinc (model 2) with the following ratio:

$$O_{NB}/Zn = [2(c_O - 2\,c_P) - N_{BO}\,c_B]/c_{Zn}. \quad (7)$$

For glasses with P_2O_5 contents of 50 mol%, model 2 predicts that O_{NB}/Zn = 4. This value is exactly what is necessary for isolated ZnO_4 units and fully tetrahedral networks (filled squares in Figure 9a). Differently, the fixed O/P ratios of 3.25 produce a continuous increase in O_{NB}/Zn with increasing B_2O_3 content (cf. Figure 9b). For completeness, the O_{NB}/Zn ratios according to model 2 for the zbp12 and zbp13 samples result in 3.10 and 3.27, respectively.

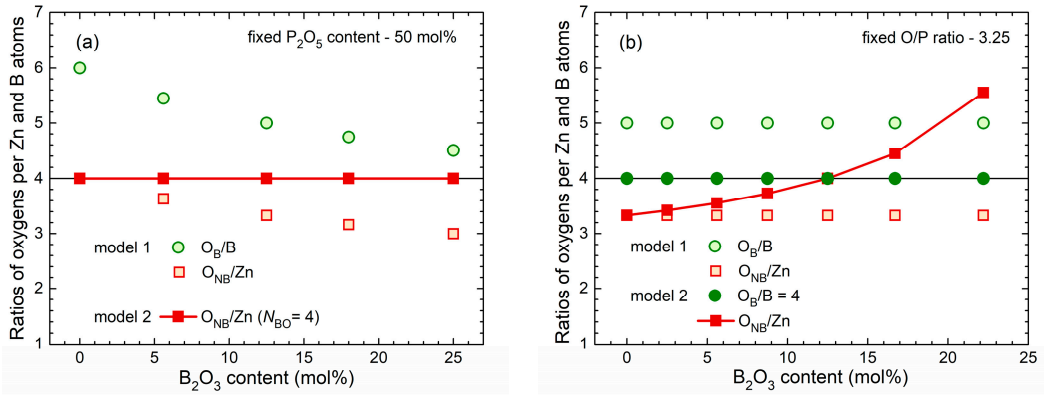

Figure 9. Ratios of the available oxygens for coordination of the Zn and B atoms for two series of the Zn borophosphate glasses with (**a**) constant P_2O_5 content of 50 mol% and (**b**) constant O/P ratio of 3.25. The models are explained in the text. To assign sample numbers, see Figure 1b. The values at 12.5 mol% B_2O_3 in (**a**,**b**) belong to the zbp09 sample.

The O_{NB}/Zn ratio becomes less than four for glasses with P_2O_5 contents below 50 mol%. Then, two ZnO_4 units must share some of their O_{NB} neighbors. The obtained O_{NB}/Zn ratios are still larger than three, which means a few connected ZnO_4 units are present, but not any interconnected ZnO_4 substructures. If one looks at the binary ZnO-B_2O_3 glasses obtained with 54 to 70 mol% ZnO [19], theO_{NB}/Zn ratios reach only 1.5 to 1.9 (Table S3). For the ZnO_4 units existing in these glasses, each O_{NB} is shared by at least

two Zn and extended substructures of interconnected ZnO_4 exist. Octahedral ZnO_6 units were proposed for these glasses [19]. However, EXAFS and X-ray scattering suggest that ZnO_4 units are the dominant moiety [43]. The N_{ZnO} value of 4.3 for our Zn borate glass is similar to those of the borophosphate glasses. Its mean bond length of 0.200 nm is the largest among those of the other glasses (cf. Figure 7c). The Zn−O distances of zbp14 show large variations due to the massive need for shared O_{NB}. Highly distorted ZnO_5 polyhedra co-exist beside ZnO_4.

Figure 9b shows strongly increasing O_{NB}/Zn ratios > 4 with increasing B_2O_3 contents. Thus, a significant increase in N_{ZnO} is forced. According to the Zn−O distances (Figures 5b and 7b), the N_{ZnO} of the zbp11 sample is significantly larger than four but it is expected to be less than five. Otherwise, in the case of $N_{ZnO} < O_{NB}/Zn$, some terminal P=O double bonds must occur. According to the other limitations of the zbp11 sample (N_{PO} = 3.6), its P_2O_5 content should be a little less than the nominal value. The formation of homogeneous glasses reaches the limit for this sample as reported for such compositions [22].

Model 1 was introduced assuming equal preferences of B and Zn for the oxygens of the different Q^n. The B and Zn would form their environments independently. However, that is not possible with the limit $N_{BO} \leq 4$. For the ZnO-Al_2O_3-P_2O_5 glasses, the Al−O coordination number can increase up to six and the changes of N_{AlO} according to model 1 are possible in a large concentration range. The N_{AlO} values were calculated from the fractions of the AlO_4, AlO_5, and AlO_6 units, which were determined with ^{27}Al MAS NMR [24]. One of the glasses is a compositional analog to that of the zbp11 sample. That Al−O coordination number was 5.2 and close to 5.0, which resulted from model 1 (Figure 9b). The structural analysis of Na_2O-Al_2O_3-P_2O_5 glasses has shown that all oxygen is used to break P−O−P bridges [44]. The compositional dependence of N_{AlO} was found to follow other rules than simply a continuous increase with the O_{NB} fractions. Abrupt changes from N_{AlO} = 4 to 6 were found [44], which indicates the greater stability of the AlO_4 and AlO_6 polyhedra if compared with the AlO_5. The Na^+ coordinating the oxygens in Al−O−P bridges is essential for this behavior. Certainly, special preferences with the different Q^n groups exist.

In this work, the different preferences for the oxygens of the Q^2, Q^1, and Q^0 units with the Zn and B polyhedra are due to the restrictions of the B to BO_4 units (model 2). The different field strengths of Zn^{2+} and B^{3+} are not essential in this context. The maximum limit N_{BO} = 4 made the model considerations comparably simple for the borophosphate glasses of this study. As long as the N_{BO} value = 4 is less than the O_B/B ratio of model 1, the O_{NB}/Zn ratio can be calculated and it determines the Zn−O environments. The success of model 2 became obvious in the predicted behavior of the Zn−O distances with the narrow peaks along the line of 50 mol% P_2O_5.

4.2. The Stabilization of the BO_4 Units and the Boron Anomaly

BO_4 tetrahedra and planar BO_3 triangles are the units in the crystalline forms of B_2O_3 [45,46]. The BO_4 unit is the variant with the densest packing and can be formed provided that its bond valences can be balanced. In the high-pressure B_2O_3 crystal [45], charge compensation is realized with oxygens which are threefold-linked to borons. Usually, glasses are only obtained when there is no or little threefold connected oxygen in the network. Accordingly, vitreous B_2O_3 forms BO_3 units. Other mechanisms can deplete electron density from the B−O bonds in the BO_4 unit resulting in four bonds with the necessary valences of ~0.75 vu. The BO_4 units in binary borate glasses were identified as the origin of non-continuous property changes known as the boron anomaly [12].

For the borophosphate glasses, the BPO_4 crystals [14,15] show the mutual benefit for the B and P atoms with a deficit and excess valence electron density in the B−O−P bridges of the tetrahedral networks (cf. Figure 8a). This type of valence transfer is effective throughout the Zn borophosphate glasses studied, whereby the BO_4 units do not form B−O−Zn bridges. The typical PO_4–Zn interactions are shown in Figure 10a,b, which were discussed above. The interaction of the Zn with the oxygen sites in P−O−B bridges is

rather improbable. Each Zn−O bond of a ZnO_4 requires a bond valence of ~0.50 vu, which is too much to be shared with these oxygens. For the same reasons, the oxygen corner of a ZnO_4 unit cannot be the oxygen between two BO_3 units or a pair of BO_3 and BO_4 (analogously to Figure 10g). These circumstances suggest a relation to the lack of glass formation in the B_2O_3-rich and P_2O_5-poor regions of the Zn borophosphate system. There is one exception; the oxygen sites in B−O−B between BO_4 pairs can coordinate a Zn (cf. Figure 10d), as found in several Zn borate crystals [47–50]. However, this feature is not sufficient to stabilize any glasses poor in P_2O_5, but it can occur in the glasses of moderate P_2O_5 content until just under 50 mol%.

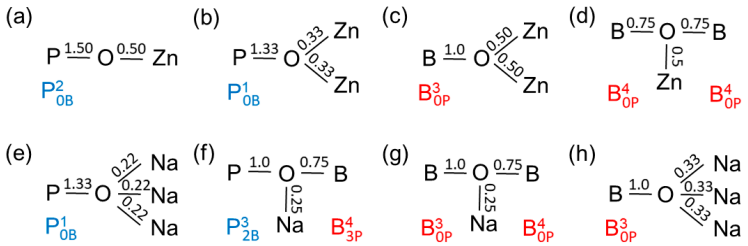

Figure 10. Characteristic modifier oxygen interactions in the Zn and Na borophosphate glasses and crystals: (**a**,**b**) one or two Zn bound to an O_{NB} (P−O_{NB}), (**c**) two Zn bound to an O_{NB} (B−O_{NB}), (**d**) Zn bound to an O_B in a B−O−B bridge ($Zn_2B_{10}O_{17}$ crystal [49]), (**e**) three Na bound to an O_{NB} (P−O_{NB}), (**f**) Na bound to an O_B in a P−O−B bridge ($Na_5B_2P_3O_{13}$ crystal [17]), (**g**) Na bound to an O_B in a B−O−B bridge ($Na_2B_8O_{13}$ crystal [51]), and (**h**) three Na bound to an O_{NB} (B−O_{NB}). The numbers indicate the bond valences given in valence units (vu).

Binary Zn borate glasses are obtained in a small range rich in ZnO [19], where a significant fraction of O_{NB} in BO_3-triangles already exists ($O_{NB}/Zn \geq 1.5$). Two Zn^{2+} cations share each O_{NB} (cf. Figure 10c), which means that at least three such O_{NB} corners are present in each Zn-O environment. The scattering results of the Zn borate glass (zbp14) suggest a fraction of ZnO_5 units in addition to the ZnO_4. The ZnO_5 have bonds of unequal lengths whose two more distant corners can coordinate the oxygens in any B−O−B bridge. The corner of a ZnO_4 can only coordinate an O_B in a bridge between two BO_4 units (cf. Figure 10d), as explained in the preceding paragraph.

Similar to the ZnO_4 units, the Na^+ cations have total coordination numbers close to four (Table S2). The cation oxygen distance is larger for Na^+ and the width (fwhm) of the Na−O peak is ~0.042 nm (cf. Figure S8), much more than the ~0.017 nm of the Zn−O peak (Figure 6). These parameters express the large flexibility of the Na^+ cations to form distorted oxygen environments. Figure 10e,h show the interaction of the Na^+ with the O_{NB} of the P or B atoms, which is similar to the Zn−O bonds in Figure 10a–c. Here, the Na-O bonds are drawn with bond valences of ~0.25 vu as belonging to a NaO_4 tetrahedron. This value can vary according to the distortions of the NaO_m polyhedron, including the variations in m. The Na−O bonds are dominantly ionic, but it is better not to mix the bond valences and electronic charges in the schematic presentations. The weak Na−O interaction allows the Na^+ to approach the O_B sites in the P−O−B and B−O−B bridges (cf. Figure 10f,g). The corresponding oxygens are still quasi-twofold linked. The third partner Na^+ forms a flexible bond that maintains sufficient flexibility to the disordered network as necessary for glass formation.

It was emphasized that the BO_4 units in the Zn borophosphate glasses with P_2O_5 contents of ≥50 mol% are charge-balanced by PO_4 units (Figure 8). The Zn^{2+} cations can approach oxygens in B−O−B bridges only for glasses with a P_2O_5 content < 50 mol% and then also contribute to the BO_4 stabilization. Of course, the BO_4 fractions in the binary Zn borate glasses [19] are charge-balanced by the Zn^{2+} cations. What about the Na borophosphate glasses? One can compare them with the known crystal structures. The $Na_2B_8O_{13}$ crystal, which is free of phosphate [51], shows two mechanisms for BO_4 stabilization through Na^+. The lengths of the B−O bonds suggest that the surplus negative

charge of the BO_4 is not only balanced by the Na^+ coordinating the BO_4 corners, but it is also transferred to the neighboring BO_3 triangles. The bond lengths in the BO_3 units are strengthened in B−O−B bridges to the BO_4 (~0.134 nm), whereas they are elongated in bridges to other BO_3 (~0.138 nm). Thus, the Na^+ cations also act across the BO_3 triangles as neighbors of the BO_4. It is to be presumed that there is no serious difference between the depletion effects of electron density from the bonds in the BO_4 in the direction of the PO_4 units or the Zn^{2+} and Na^+ cations.

4.3. Different Effects of Zn and Na on the P−O Bond Lengths

The lengths of the P−O bonds in the zbp13 and nbp13 glasses with compositions with an O/P ratio of 3.5 reveal different effects of the Zn^{2+} and Na^+ cations. Binary phosphate glasses with the same O/P ratio (pyrophosphates with O_{NB}/O_B = 6:1) possess two different lengths of P−O bonds, the P−O_{NB} and P−O_B bonds, with a frequency ratio of 3:1 [23,36]. The obtained distribution of bond lengths of a corresponding glass ($ZnPbP_2O_7$ [36]) is shown in Figure 11, and its structure is illustrated in Figure S9a.

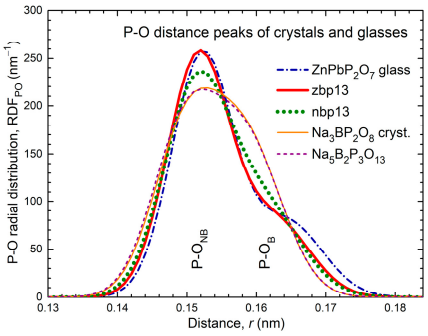

Figure 11. The model peaks of the P−O bond lengths of the zbp13 and nbp13 samples are compared to the P−O distances of a $(ZnO)_{0.10}(PbO)_{0.56}(P_2O_5)_{0.34}$ glass [36] with the same O/P ratio = 3.5. A numeral ratio of 3:1 is effective for the P−O_{NB} and P−O_B bonds of a phosphate glass with this O/P. The bonds are indicated in the figure. The Zn borophosphate glass shows a similar behavior in its bond lengths. Regarding the Na borophosphate glass and the crystals $Na_3BP_2O_8$ and $Na_5B_2P_3O_{13}$ [16,17], some P−O bonds in the P−O−B bridges reach lengths typical for the P−O_B bonds in P−O−P bridges. The five curves have been given equal areas.

The neutron diffraction results of zbp13 and nbp13 also show two types of P−O bonds (cf. Figures S3 and S4). The frequency numbers of the two P−O bonds are obtained with 2.8 and 1.0 for zbp13 and 2.5 and 1.3 for nbp13 (cf. Table S2). The corresponding ratios of bonds are similar to that of the $ZnPbP_2O_7$ glass, though the P−O_{NB}/P−O_B ratios of 9:11 for zbp13 and nbp13 are formally quite different from 3:1 (cf. Figure S9). This difference is explained by short P−O_B bonds in the P−O−B bridges if compared with those in the P−O−P bridges.

For the zbp13 sample, the ratio is close to 3:1, and the P−O peak agrees with that of the $ZnPbP_2O_7$ glass (cf. Figure 11). The nbp13 sample has a slightly larger fraction of P−O bonds with lengths of ~0.160 nm. An effect that could increase this P−O fraction is the formation of B−O−B bridges between two BO_4 according to Equation (4), which is accompanied by additional P−O−P bridges. A borophosphate glass with a composition close to that of zbp13 has 27.7% boron in B^4_{3P} units [13]. According to the glass composition of zbp13 and excluding B−O−B bridges, the P−O bonds can be divided into 25% in P−O−P bridges, 30% in P−O−B bridges, and 45% in P−O_{NB}. A total of 27.7% of the B in B^4_{3P} units means that there is an increase in the bonds in P−O−P bridges from 25% to 27%. Therefore, the corresponding increase in the number of longer P−O_B bonds is insignificant (<0.1).

The Na borophosphate glass nbp13 is expected to be almost free of B−O−B bridges, as has been reported for a similar glass (sample x = 0.125 in [10]). The structures of the

$Na_3BP_2O_8$ [16] and $Na_5B_2P_3O_{13}$ [17] crystals help to understand the larger fraction of the longer P−O bonds, although the crystal's compositions differ somewhat from that of nbp13 (cf. Figure 1). The Na borophosphate crystals have isolated PO_4 units (Q^0). From the point of view of binary phosphates [23], only a single P−O distance should occur. However, two distances become obvious (cf. Figure 11). Half of the oxygens of the PO_4 units participate in P−O−B bridges and these oxygens have a Na^+ cation in their close vicinity, as illustrated in Figure 10f. These Na^+ stabilize the BO_4 but also reduce the bond valence in the adjacent PO_4 (elongation of the P−O bond). The other two PO_4 corners coordinate only Na^+ cations, as shown in Figure 10e, and the corresponding short P−O bonds carry the surplus bond valence taken over from the others. The difference in both P−O bond strengths in these crystals is a little smaller than that in the zbp13 and $ZnPbP_2O_7$ glasses, the latter with bond valences of 1.33 and 1.0 vu (cf. Figure 11). For the nbp13 glass, the changes in bond lengths appear less pronounced than in the crystals. Again, 25% of the P−O bonds are in P−O−P bridges, 30% in P−O−B bridges, and 45% in $P-O_{NB}$. To achieve the right ratio of the short and long P−O bonds of the nbp13 sample (2.5:1.3), the fraction of the P−O−B bridges is split into two parts, those with a Na^+ close nearby and those free of any Na^+ neighbor. Then, 30% of the P−O bonds in the P−O−B bridges are elongated, indicating the effect of a Na^+ cation. The other 70% of P−O bonds in P−O−B bridges are not affected by any Na^+ cations and have lengths similar to those of typical $P-O_{NB}$ bonds. This difference from zbp13 means that the BO_4 units in the nbp13 glass undergo charge compensation equally by Na^+ cations and PO_4 units. The ZnO_4 units in zbp13 contribute less because their corners do not participate in P−O−B bridges.

Two species of P−O−B bridges are suggested for nbp13 that seem to be easily distinguishable. One is coordinated to a Na^+ cation, and the other is not. On the other hand, a clear separation of the P−O−B bridges into those with and without a Na^+ neighbor might be questionable due to the large width of the Na−O distance peak. Both P−O peak components overlay with each other. The analyses of the O 1s spectra (XPS) did not distinguish two different types of P−O−B bridges in the Na and Zn borophosphate glasses [8,20]. Nevertheless, the effect of the Na^+ on the P−O−B is real and it is not effective for Zn^{2+}. Another approach supports the fact that only part of the P−O−B bridges of nbp13 can have Na^+ neighbors. The total Na−O coordination number is calculated assuming all oxygens in the $P-O_{NB}$ bonds or P−O−B bridges are present with three or one Na^+ neighbors, as shown in Figure 10e,f, respectively. Then, for nbp13, a N_{NaO} value of ~6.0 is obtained, which noticeably exceeds the value of 4.0 obtained from scattering. Accordingly, only part of the P−O−B can have a Na^+ neighbor (30% as estimated for nbp13). Also, the O_{NB} shown in Figure 10e can only have 2.3 Na^+ neighbors on average instead of 3 Na^+ neighbors. These conditions mean that only a third of the Na^+ can coordinate the oxygen in a P−O−B bridge. All other oxygens in the Na−O bonds belong to the $P-O_{NB}$ bonds. Here, only the behavior of a single sample is discussed. The corresponding relations will strongly change with the glass compositions.

The ionic forces of Na^+ are weak compared to strong P−O and B−O bonds. Therefore, Na^+ does not form dense oxygen environments, e.g., NaO_6 octahedra. The broad Na−O distance peaks (cf. Figure S8) correspond to N_{NaO} values of 4.5 and 4.0 in the glasses and are thus significantly smaller than those (5 and 6) in the related crystals [16,17], accompanied by shorter bonds. Likewise, the number and bond valences of the $P-O_{NB}$ bonds in zbp13 (cf. Figure 10b) would allow the Zn^{2+} to form ZnO_6 octahedra, which is not the case. The strong bonds in the PO_4 and BO_4 units and the comparatively high cross-linking density of the borophosphate networks prevent the modifier cations from forming compact oxygen polyhedra.

The relation between the network structure and the modifier environments was also used to interpret the mixed network-former effect. The average number of O_B per glass-forming unit, *BO*, calculated for the $y Na_2O$-$x B_2O_3$-$(1-x)P_2O_5$ glasses, characterizes the stiffness of the network [6,10]. This value's behavior correlates well with the T_g values. A larger *BO* means an increasing network stiffness, which is accompanied by more disordered

modifier environments; in this case, it is the NaO_m polyhedron. In addition, the O_{NB}/Na ratio decreases (Equation (7)). These changes explain the reduced activation energies for ionic transport when the B_2O_3 content increases while the Na_2O content is constant [6,10]. The average number of bridging corners per network-forming unit, BC_{NFU}, is a more plausible value with $BC_{NFU} = 2\ BO$. For the borophosphate glasses, it is calculated with the following:

$$BC_{NFU} = 2(4c_P + N_{BO}\ c_B - c_O)/(c_P + c_B)\ . \quad (8)$$

The BC_{NFU} value is two for the P^2_{0B} chain units in the $NaPO_3$ glass. It increases to 2.6 for the nbp13 sample. Maximum values of $\geq$3 are reached for a larger B_2O_3 content until the potential of the PO_4 units to stabilize the BO_4 is exhausted and BO_3 triangles occur. The Na−O distances of the two glass compositions are shown in Figure S8. A significant change in the Na−O peaks is not observed. The small scattering power of Na, if compared with Zn and the overlap with the O−O distances at 0.25 nm, impede an accurate distance analysis.

Previous diffraction work on Na_2O-B_2O_3-P_2O_5 glasses [52,53] did not reach such a large Q_{max}, which is needed to resolve different P−O bonds. The structural analysis was made using the Reverse Monte Carlo (RMC) technique, which aimed to elucidate the mixed network-former effect. A main point was the description of the medium-range order which includes the migration pathways for the Na^+ cations. The analysis of the Na−O environments in the model configurations gave total N_{NaO} values of ~4.5 with very broad distributions of the distinct Na sites ranging from a two- to eightfold coordination. The two distances of 0.152 and 0.156 nm given in [53] for the P−O_{NB} and P−O_B bonds are simply calculated from the RMC configurations, but are not resolved in the measuring results and thus cannot be compared with our data.

4.4. The Evolution of the Properties of the Zn Borophosphate Glasses

The figures with the mass densities ρ of the ZnO-B_2O_3-P_2O_5 glasses in [22] show a continuous increase with fixed ZnO and increasing B_2O_3 contents. Glass transition temperatures T_g show similar trends while the expansion coefficients α change in opposite directions. The values of ρ and T_g in [13] show similar trends, although the comparisons are made along constant O/P ratios. It needs to be remembered that the Zn phosphate glasses have been classified as showing anomalous behavior [40]. The minima of mass density at 50 mol% ZnO [25,40,54] or T_g values [13,54] at ~60 mol% ZnO are characteristic of the binary Zn phosphate glasses. Below, the mass densities that were published for the full range of glass formation in the ZnO-B_2O_3-P_2O_5 system are discussed [22]. Packing densities are better suited for comparisons whereby the influence of atomic size and mass is widely eliminated. Such comparisons were made for the ZnO-P_2O_5 glasses recently [27] by using the ionic radii from [55].

A packing density is the filled volume fraction, assuming the atoms are spheres of known ionic radii. Since the BO_4 tetrahedra have small O−O distances, there is some overlap of the oxygen spheres with an ionic radius of 0.135 nm; to a lesser extent, there is also some overlap for the PO_4 tetrahedra. A correction was made for this overlap. The packing densities of the Zn borophosphate glasses obtained from the mass densities given in [22] are shown in Figure 12 as numbers given close to the sample positions in the concentration triangle. The absolute minimum at 50 mol% ZnO shows a packing density of 46.4%. This behavior was attributed to being caused by the network of corner-connected PO_4 and ZnO_4 tetrahedra with all oxygens in bridges (Figure 8b), a network that fills the space quite inefficiently [25].

Above, it was shown that the tetrahedral character of the network does not change when B_2O_3 replaces the ZnO while 50 mol% P_2O_5 is fixed. A plateau of ~51% packing density is reached with 10% B_2O_3 (Figure 12). This increase is due to the exchange of the rather open ZnO_4 unit for the more compact BO_4 unit. There exists a further subtle increase in the packing density up to ~52.5% in the direction of decreasing P_2O_5 contents. This fact is interpreted with the change from P−O−Zn bridges (Figure 10a) to the first O_{NB} shared by two Zn (Figure 10b) and the exchange of PO_4 for BO_4 units. Finally, when only isolated PO_4

units exist, then BO_3 units with O_{NB} shared by two Zn are also formed (Figure 10c), and the packing densities still increase. The $(ZnO)_x(B_2O_3)_{1-x}$ glasses with $0.54 \leq x \leq 0.67$ [19] with few BO_4 connected with BO_3 have packing efficiencies of 55% to 53.5%, where the O_{NB} of the BO_3 are shared by two Zn. For the reachable glass compositions, the BO_3 units of the Zn borate glasses have one or two O_{NB}.

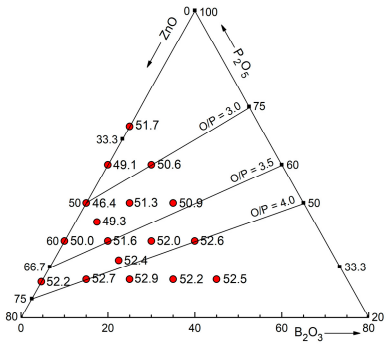

Figure 12. The packing densities of the ZnO-B_2O_3-P_2O_5 glasses obtained from the mass densities given in [22] are given as numbers near the sample positions in the concentration triangle of the three components. The values of the packing densities are given in percent.

5. Conclusions

The atomic structures of Zn and Na borophosphate glasses were investigated using scattering methods. Neutron scattering was successfully performed on glasses with up to 8% boron atoms, which contains the strongly absorbing ^{10}B isotope in natural abundance. The X-ray scattering of high-energy photons using the image plate technique was crucial for determining the Zn−O distances. Neutron scattering at the spallation source offered a large measuring range (large Q_{max}), which is a prerequisite for the high resolving power of pair distances. Detailed analyses of different lengths of P−O bonds became possible.

The Zn−O coordination numbers were found to be a little larger than four and did not change significantly when changing the glass compositions. What is striking, however, is that the glasses along a line connecting the BPO_4 and $Zn(PO_3)_2$ compositions (50 mol% P_2O_5) showed the narrowest peaks of Zn−O distances. This indicates the formation of tetrahedral networks of PO_4, BO_4, and ZnO_4 with mostly isolated ZnO_4 units and no B−O−Zn bridges. The calculated amount of the O_{NB} that is available for the Zn−O coordination supports this interpretation. For smaller P_2O_5 contents, the Zn share O_{NB} which leads to distances of ~0.212 nm and thus, a broadening of the Zn−O peaks. The one sample of a P_2O_5 content larger than 50 mol% shows a subtle increase in N_{ZnO} that is accompanied by a broadened Zn−O peak as well. The two investigated Na borophosphate glasses have Na−O distances similar to those of a $NaPO_3$ glass with coordination numbers of 4 to 4.5, while NaO_5 and NaO_6 polyhedra exist in the related crystals with Na−O distances that are a little larger. The first-neighbor distances of the B−O, P−O, and O−O pairs in the real-space correlations confirm that only BO_4 units co-exist with the PO_4 in the borophosphate networks.

Two peaks of P−O bonds are visible for the binary phosphate glasses, which has been commonly observed. They are assigned to the short P−O_{NB} bonds and the longer P−O_B bonds. This behavior also exists for the ZnO-B_2O_3-P_2O_5 glasses whereby, however, the first peak component includes the ordinary P−O_{NB} bonds together with the bridging bonds of the P−O−B linkages, according to their similar lengths. Though some B−O−B bridges exist, the concomitant increase in the fraction of the longer P−O_B bonds is small. On the other hand, significantly larger fractions of the long P−O_B bonds are found for the Na_2O-B_2O_3-P_2O_5 glasses. Some Na^+ cations coordinate oxygens in a part of the P−O−B bridges which elongates the corresponding P−O bonds. Thus, BO_4 units formed in the Zn borophosphate glasses are charge-balanced by mainly PO_4 units while the charge balance

of the BO_4 in the Na borophosphate glasses is realized by the neighboring PO_4 and the Na^+ cations equally.

The property changes of the ZnO-B_2O_3-P_2O_5 glasses seem to be complex. The changes with the B_2O_3 additions interfere with the known anomalies of the ZnO-P_2O_5 glasses that have a minimum packing density at 50 mol% and a minimum glass transition temperature at ~40 mol% P_2O_5.

Supplementary Materials: The following supporting information can be downloaded at: https://www.mdpi.com/article/10.3390/solids5030024/s1, Figure S1: X-ray structure factors; Figure S2: X-ray correlation functions zbp14; Figure S3: Neutron and X-ray correlation functions zbp07, zbp11, and zbp13; Figure S4: Neutron and X-ray correlation functions nbp13; Figure S5: Zn−O coordination numbers; Figure S6: Fractions of the long Zn−O bonds; Figure S7: Rearrangements of network groups; Figure S8: Na−O first-neighbor distances; Figure S9: Structural illustrations; Table S1: Batch compositions and mass densities; Table S2: Parameters of the model Gaussian peaks; Table S3: Parameters of the Zn borate glasses [19].

Author Contributions: Conceptualization, U.H. and R.K.B.; methodology, P.T.F., J.B., U.H. and A.C.H.; formal analysis, U.H.; investigation, P.T.F. and U.H.; resources, R.K.B., J.B. and A.C.H.; writing—original draft preparation, U.H.; writing—review and editing, R.K.B. All authors have read and agreed to the published version of the manuscript.

Funding: This research received no external funding.

Data Availability Statement: The data are available upon request.

Conflicts of Interest: The authors declare no conflicts of interest.

References

1. Ray, N.H. *Inorganic Polymers*; Academic Press: London, UK, 1978; pp. 79–90.
2. Sharmin, N.; Hasan, M.S.; Parsons, A.J.; Furniss, D.; Scotchford, C.A.; Ahmed, I.; Rudd, C.D. Effect of boron addition on the thermal, degradation, and cytocompatibility properties of phosphate-based glasses. *BioMed Res. Int.* **2013**, *2013*, 902427. [CrossRef] [PubMed]
3. Petit, L.; Cardinal, T.; Videau, J.J.; Smektala, F.; Jouan, T.; Richardson, K.; Schulte, A. Fabrication and characterization of new Er^{3+} doped niobium borophosphate glass fiber. *Mater. Sci. Eng. B* **2005**, *117*, 283–286. [CrossRef]
4. Chiodelli, G.; Magistris, A.; Villa, M. Ionic conductivity and glass transition of borophosphate glasses. *Solid State Ion.* **1986**, *18–19*, 356–361. [CrossRef]
5. Christensen, G.; Olson, G.; Martin, S.W. Ionic conductivity of mixed glass former $0.35Na_2O + 0.65[xB_2O_3 + (1 - x)P_2O_5]$ glasses. *J. Phys. Chem. B* **2013**, *117*, 16577–16586. [CrossRef]
6. Zielnok, D.; Cramer, C.; Eckert, H. Structure/property correlations in ion-conducting mixed-network former glass: Solid-state NMR studies of the system Na_2O-B_2O_3-P_2O_5. *Chem. Mater.* **2007**, *19*, 3162–3170. [CrossRef]
7. Carta, D.; Qiu, D.; Guerry, P.; Ahmed, I.; Abou Neel, E.A.; Knowles, J.C.; Smith, M.E.; Newport, R.J. The effect of composition on the structure of sodium borophosphate glasses. *J. Non-Cryst. Solids* **2008**, *354*, 3671–3677. [CrossRef]
8. Raskar, D.; Rinke, M.T.; Eckert, H. The mixed-network former effect in phosphate glasses: NMR and XPS studies of the connectivity distribution in the glass system $(NaPO_3)_{1-x}(B_2O_3)_x$. *J. Phys. Chem. C* **2008**, *112*, 12530–12539. [CrossRef]
9. Muñoz, F.; Montagne, L.; Pascual, L.; Durán, A. Composition and structure dependence of the properties of lithium borophosphate glasses showing boron anomaly. *J. Non-Cryst. Solids* **2009**, *355*, 2571–2577. [CrossRef]
10. Larink, D.; Eckert, H.; Reichert, M.; Martin, S.W. Mixed network former effect in ion-conducting alkali borophosphate glasses: Structure/property correlations in the system $[M_2O]_{1/3}[(B_2O_3)_x(P_2O_5)_{1-x}]_{2/3}$ (M = Li, K, Cs). *J. Phys. Chem. C* **2012**, *116*, 26162–26176. [CrossRef]
11. Christensen, R.; Olson, G.; Martin, S.W. Structural studies of mixed glass former $0.35Na_2O + 0.65[xB_2O_3 + (1 - x)P_2O_5]$ glasses by Raman and ^{11}B and ^{31}P Magic Angle Spinning Nuclear Magnetic Resonance spectroscopies. *J. Phys. Chem. B* **2013**, *117*, 2169–2179. [CrossRef]
12. Krogh-Moe, J. *On the Structure of Boron Oxide and Alkali Borate Glasses*; Doktorsavhandlingar vid Chalmers Tekniska Högskola Nr. 22: Göteborg, Sweden, 1959.
13. Freudenberger, P.T.; Brow, R.K. Spectroscopic and chromatographic analyses of zinc borophosphate glasses. *Phys. Chem. Glas. B* **2018**, *59*, 227–284.
14. Haines, J.; Cambon, O.; Astier, R.; Fertey, P.; Chateau, C. Crystal structures of α-quartz homeotypes boron phosphate and boron arsenate: Structure-property relationships. *Z. Krist.* **2004**, *219*, 32–37. [CrossRef]
15. Haines, J.; Chateau, C.; Léger, J.M.; Bogicevic, C.; Hull, S.; Klug, D.D.; Tse, J.S. Collapsing cristobalitelike structures in silica analogues at high pressure. *Phys. Rev. Lett.* **2003**, *91*, 015503. [CrossRef]

16. Bang, X.D.; Hong, C.H.; Xin, Y.X.; Thai, Z.J. Low-temperature flux syntheses and characterizations of two 1-D anhydrous borophosphates: $Na_3B_6PO_{13}$ and $Na_3BP_2O_8$. *J. Solid State Chem.* **2007**, *180*, 233–239.
17. Hauf, C.; Friedrich, T.; Kniep, R. Crystal structure of pentasodium catena-(diborato-triphosphate), $Na_5B_2P_3O_{13}$. *Z. Kristallogr.* **1995**, *210*, 446. [CrossRef]
18. Zhang, E.; Zhao, S.; Zhang, J.; Fu, P.; Yao, J. The β-modification of trizinc borate phosphate, $Zn_3(BO_3)(PO_4)$. *Acta Crystallogr. E* **2001**, *67*, i3. [CrossRef] [PubMed]
19. Topper, B.; Möncke, D.; Youngman, R.E.; Valvi, C.; Kamitsos, E.I.; Versamis, C.P.E. Zinc borate glasses: Properties, structure and modelling of the composition-dependence of borate speciation. *Phys. Chem. Chem. Phys.* **2023**, *25*, 5967–5988. [CrossRef]
20. Brow, R.K. An XPS study of oxygen bonding in zinc phosphate and zinc borophosphate glasses. *J. Non-Cryst. Solids* **1996**, *194*, 267–273. [CrossRef]
21. Brow, R.K.; Tallant, D.R. Structural design of sealing glasses. *J. Non-Cryst. Solids* **1997**, *222*, 396–406. [CrossRef]
22. Koudelka, L.; Mošner, P. Borophosphate glasses of the $ZnO-B_2O_3-P_2O_5$ system. *Mater. Lett.* **2000**, *42*, 194–199. [CrossRef]
23. Brow, R.K. Review: The structure of simple phosphate glasses. *J. Non-Cryst. Solids* **2000**, *263–264*, 1–28. [CrossRef]
24. Smith, C.E.; Brow, R.K.; Montagne, L.; Revel, B. The structure and properties of zinc aluminophosphate glasses. *J. Non-Cryst. Solids* **2014**, *386*, 105–114. [CrossRef]
25. Hoppe, U.; Walter, G.; Kranold, R.; Stachel, D.; Barz, A. The dependence of structural peculiarities in binary phosphate glasses on their network modifier content. *J. Non-Cryst. Solids* **1995**, *192–193*, 28–31. [CrossRef]
26. Hoppe, U.; Walter, G.; Stachel, D.; Barz, A.; Hannon, A.C. Neutron and X-ray diffraction study on the structure of ultraphosphate glasses. *Z. Naturforsch. A* **1997**, *52*, 259–269. [CrossRef]
27. Hoppe, U. The oxygen environments of divalent cations in phosphate glasses and crystals—The change with composition and ionic radii. *J. Non-Cryst. Solids* **2023**, *619*, 122599. [CrossRef]
28. Bionducci, M.; Licheri, G.; Musinu, A.; Navarra, G.; Piccaluga, G.; Pinna, G. The structure of Zn(II) metaphosphate glass. *Z. Naturforsch. A* **1996**, *51*, 1209–1215. [CrossRef]
29. Xia, Y.; Chen, H.; Hung, I.; Gan, Z.; Sen, S. Structure and fragility of Zn-phosphate glasses: Results from multinuclear NMR spectroscopy and calorimetry. *J. Non-Cryst. Solids* **2022**, *580*, 121395. [CrossRef]
30. Dippel, A.-C.; Liermann, H.-P.; Delitz, J.T.; Walter, P.; Schulte-Schrepping, H.; Seeck, O.H.; Franz, H. Beamline P02.1 at PETRA III for high-resolution and high-energy powder diffraction. *J. Synchrotron Radiat.* **2015**, *22*, 675–687. [CrossRef]
31. Waasmaier, D.; Kirfel, A. New analytical scattering-factor functions for free atoms and ions. *Acta Crystallogr. A* **1995**, *51*, 416–431. [CrossRef]
32. Hubbell, J.H.; Veigele, W.J.; Briggs, E.A.; Brown, R.T.; Cromer, D.T.; Howerton, R.J. Atomic form factors, incoherent scattering functions, and photon scattering cross sections. *J. Phys. Chem. Ref. Data* **1975**, *4*, 471–538. [CrossRef]
33. Hannon, A.C. Results on disordered materials from the GEneral Materials diffractometer, GEM, at ISIS. *Nucl. Instrum. Methods Phys. Res. Sect. A* **2005**, *551*, 88–107. [CrossRef]
34. Leadbetter, A.J.; Wright, A.C. Diffraction studies of glass structure: I. Theory and quasi-crystalline model. *J. Non-Cryst. Solids* **1972**, *7*, 23–26. [CrossRef]
35. Hannon, A.C. Neutron diffraction techniques for structural studies of glasses. In *Modern Glass Characterization*; Affatigato, M., Ed.; John Wiley & Sons: Hoboken, NJ, USA, 2015; p. 190ff.
36. Hoppe, U.; Kranold, R.; Stachel, D.; Barz, A.; Hannon, A.C. Variation in P-O bonding in phosphate glasses—A neutron diffraction study. *Z. Naturforsch. A* **2000**, *55*, 369–380. [CrossRef]
37. Weil, M. The high-temperature modification of zinc catena-polyphosphate, β-$Zn(PO_3)_2$. *Acta Crystallogr. C* **2004**, *60*, i20–i22. [CrossRef] [PubMed]
38. Robertson, B.E.; Calvo, C. Crystal structure of α-$Zn_2P_2O_7$. *J. Solid State Chem.* **1970**, *1*, 120–133. [CrossRef]
39. Bataille, T.; Benard-Rocherulle, P.; Louer, D. Thermal behavior of zinc phenylphosphonate and structure determination of g-$Zn_2P_2O_7$ from X-ray powder diffraction data. *J. Solid State Chem.* **1998**, *140*, 62–70. [CrossRef]
40. Kordes, E.; Vogel, W.; Feterowsky, R. Physikalisch-chemische Untersuchungen über die Eigenschaften und den Feinbau von Phosphatgläsern. *Z. Elektrochem.* **1953**, *57*, 282–289. [CrossRef]
41. Krause, J.T.; Kurkjian, C.R. Vibrational anomalies in inorganic glass formers. *J. Am. Ceram. Soc.* **1968**, *51*, 226–227. [CrossRef]
42. Hoppe, U. A structural model for phosphate glasses. *J. Non-Cryst. Solids* **1995**, *195*, 138–147. [CrossRef]
43. Kajinami, A.; Harada, Y.; Inoue, S.; Deki, S.; Umesaki, N. The structural analysis of zinc borate glass by laboratory EXAFS and X-ray diffraction measurements. *Jpn. J. Appl. Phys.* **1999**, *38* (Suppl. 1), 132–135. [CrossRef]
44. Brow, R.K.; Kirkpatrick, R.J.; Turner, G.L. Nature of alumina in phosphate glasses: II, structure of sodium aluminophosphate glass. *J. Am. Ceram. Soc.* **1993**, *76*, 919–928. [CrossRef]
45. Prewitt, C.T.; Shannon, R.D. Crystal structure of a high-pressure form of B_2O_3. *Acta Crystallogr. B* **1968**, *24*, 869–874. [CrossRef]
46. Gurr, G.E.; Montgomery, P.W.; Knutson, C.D.; Gorres, B.T. The crystal structure of trigonal diboron trioxide. *Acta Crystallogr. B* **1970**, *26*, 906–915. [CrossRef]
47. Martinez-Ripoli, M.; Martinez-Carrera, S.; Garcia-Blanco, S. he crystal structure of zinc diborate, ZnB_4O_7. *Acta Crystallogr. B* **1971**, *27*, 672–677. [CrossRef]
48. Bondareva, O.S.; Egorov-Tismenko, Y.K.; Simonov, M.A.; Belov, N.V. Refined crystal structure of cubic skeletov zinc borate $Zn_4O[B_6O_{12}]$. *Dokl. Akad. Nauk. SSSR* **1978**, *241*, 815–817.

49. Ziegler, R.; Purtscher, F.R.S.; Bayarjargal, L.; Hofer, T.S.; Huppertz, H. The new non-centrosymmetric zinc borate $Zn_2B_{10}O_{17}$ with a unique crystal structure. *Z. Anorg. Allg. Chem.* **2023**, *649*, e202300093. [CrossRef]
50. Ziegler, R.; Seibald, M.; Stoll, C.; Huppertz, H. Synthesis and crystal structure of the zinc borate $Zn_3B_4O_9$. *Eur. J. Inorg. Chem.* **2023**, *26*, e2023000174. [CrossRef]
51. Hyman, A.; Perloff, A.; Mauer, F.; Block, S. The crystal structure of sodium tetraborate. *Acta Crystallogr.* **1967**, *22*, 815–821. [CrossRef]
52. Le Roux, S.; Martin, S.; Christensen, R.; Ren, Y.; Petkov, V. Three-dimensional structure of multicomponent $(Na_2O)_{0.35}[(P_2O_5)_{1-x}(B_2O_3)_x]_{0.65}$ glasses by high-energy X-ray diffraction and constrained reverse Monte Carlo simulations. *J. Phys. Condens. Matter* **2011**, *23*, 035403. [CrossRef]
53. Karlsson, M.; Schuch, M.; Christensen, R.; Maass, P.; Martin, S.W.; Imberti, S.; Matic, A. Structural origin of the mixed glass former effect in sodium borophosphate glasses investigated with neutron diffraction and reverse Monte Carlo modeling. *J. Phys. Chem. C* **2015**, *119*, 27275–27283. [CrossRef]
54. Brow, R.K.; Tallant, D.R.; Myers, S.T.; Phifer, C.C. The short-range structure of zinc polyphosphate glass. *J. Non-Cryst. Solids* **1995**, *191*, 45–55. [CrossRef]
55. Shannon, R.D.; Prewitt, C.T. Effective ionic radii in oxides and fluorides. *Acta Crystallogr. B* **1969**, *25*, 925–946. [CrossRef]

Disclaimer/Publisher's Note: The statements, opinions and data contained in all publications are solely those of the individual author(s) and contributor(s) and not of MDPI and/or the editor(s). MDPI and/or the editor(s) disclaim responsibility for any injury to people or property resulting from any ideas, methods, instructions or products referred to in the content.